ACS OMEGA

http://pubs.acs.org/journal/acsodf

Article

Biocompatible Nanodiamonds Derived from Coal Washery Rejects: Antioxidant, Antiviral, and Phytotoxic Applications

Anusuya Boruah, Kallol Roy, Ashutosh Thakur, Saikat Haldar, Rituraj Konwar, Prasenjit Saikia, and Binoy K. Saikia*

Cite This: *ACS Omega* 2023, 8, 11151−11160

Read Online

ACCESS | Metrics & More | Article Recommendations

ABSTRACT: Coal washery rejects (CWRs) are a major byproduct produced in coal washery industries. We have chemically derived biocompatible nanodiamonds (NDs) from CWRs toward a wide range of biological applications. The average particle sizes of the derived blue-emitting NDs are found to be in the range of 2−3.5 nm. High-resolution transmission electron microscopy of the derived NDs depicts the crystalline structure with a *d*-spacing of 0.218 nm, which is attributed to the 100 lattice plane of a cubic diamond. The Fourier infrared spectroscopy, zeta potential, and X-ray photoelectron spectroscopy (XPS) data revealed that the NDs are substantially functionalized with oxygen-containing functional groups. Interestingly, the CWR-derived NDs exhibit strong antiviral properties (high inhibition of 99.3% with an IC_{50} value of 7.664 μg/mL) and moderate antioxidant activity that widen the possibility of biomedical applications. In addition, toxicological effects of NDs on the wheatgrass seed germination and seedling growth showed minimal inhibition (<9%) at the highest tested concentration of 300.0 μg/mL. The study also provides intriguing prospects of CWRs for the creation of novel antiviral therapies.

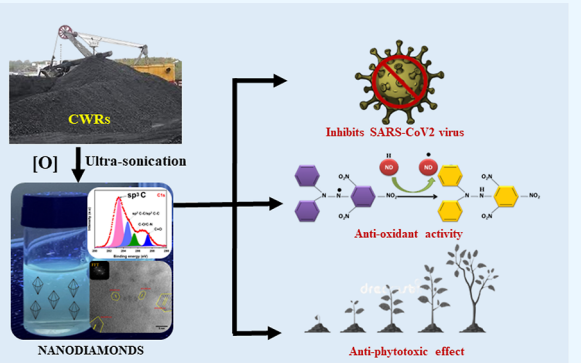

1. INTRODUCTION

Coal washery rejects (CWRs) are the solid wastes such as coal fines, rock, and soil produced worldwide as leftover materials from washing the run-off-mine (ROM) coal in coal washery industries. These coal rejects are not properly utilized and usually dumped near the sites of coal washery industries which may pollute the nearby areas.[1] The novelty of the present research work is the conversion of coal washery rejects (CWRs) into high-valued nanodiamonds (NDs) using an environmentally friendly and economically viable ultrasonic-assisted wet chemical oxidation method, holding great promise for the profitable utilization of these coal industry-generated waste materials along with possible control of the associated pollution.

NDs represent an emerging class of carbon-based nanomaterials featured with nanosized particle dimension, a crystalline diamond core within amorphous carbon layers and oxygenic functional groups on the surfaces. It has a wide range of applications including in biological fields. The unique structural characteristics account for the inherent biocompatibility,[2] superior colloidal dispersibility,[3] and stable fluorescence of NDs,[4] in addition to their primitive diamond-like properties, such as extreme hardness, abrasive nature, superior thermal conductivity, and high electrical and chemical resistance. After the discovery of the first synthetic artificial method,[5] NDs have become a topic of intense research owing to their special applications compared to other contemporary nanomaterials.[6−8] NDs are used as coating agents for metal surfaces,[9] additives for lubricant oils,[10] nanofillers for wear-resistant polymers,[11] grain refining agents in alloy formation,[12] and so forth. More recently, NDs have been established as attractive candidates for biological and medical applications, notably for therapy, drug delivery, biomedical imaging,[13] and bio-sensing.[14] Accordingly, NDs are considered the next game-changing materials for nanotechnology developments.

Many bottom-up and top-down methods have been developed for the synthesis of NDs that include the detonation of carbon-containing explosives (TNT, RDX, etc.) at high temperatures and pressure under anaerobic conditions,[15] chemical vapor deposition (CVD),[16] microplasma-assisted dissociation of ethanol vapor at atmospheric pressure,[17] chlorination of carbides,[18] ion irradiation of graphite,[19] pulsed laser ablation method (PLA),[20] ultrasound cavitation,[21] high-

Received: December 15, 2022
Accepted: March 2, 2023
Published: March 14, 2023

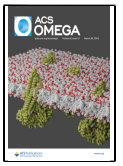

energy ball milling of diamond microcrystals grown at high pressure and temperature (HPHT),[22] and so forth. Among different methods, only energy-intensive detonation methods are available for the industrial-scale production of NDs. On the other hand, these detonation methods require highly sophisticated equipment, severe synthesis conditions, and time-consuming purification steps to produce pure NDs, making it extremely necessary to search for other sustainable routes to meet the worldwide demand for these high-impact nanodiamond (ND) materials. Therefore, there is need for a simple process for synthesis of NDs from the precursors.

Coal is the least expensive and abundantly available feedstock for fabricating carbonaceous nanomaterials. Several research groups, including ours, have reported the synthesis of numerous carbon nanomaterials, such as carbon nanotubes, onion-like fullerenes, carbon quantum dots, turbostratic graphene, graphene oxide, as well as NDs from coal feedstock.[23−25] The formation of nanocrystalline diamond (NCD) from amorphous carbon materials as a consequence of hydrogen evolution during the high-energy reactive ball milling of anthracite coal with cyclohexene was first reported by Lueking et al.[26] In a subsequent paper, it is also reported the formation of a more thermodynamically stable NCD after reactive ball milling of anthracite coal with cyclohexene and then thermal activation by high-temperature (1400 °C) annealing and finally chemical activation by treatment with an acid and a base (4 M HCl and 10 M NaOH).[27] Sun et al.[28] reported electron-beam-induced recrystallization of the carbon network of anthracite coal functionalized with dodecyl groups into NDs. Xiao et al.[29] reported the synthesis of NDs from three different coal samples by a process involving laser ablation in liquid under ambient conditions. In addition, our group also reported a simpler and more straightforward method of ND formation from low-grade Indian coals by low-power ultrasonic-assisted exfoliation of coals using hydrogen peroxide (H_2O_2) as a green oxidizing and exfoliating agent followed by purification with the dialysis process. The said low-power ultrasonic-assisted wet chemical oxidation method has been successfully used to produce ND-like materials, even from carbonaceous aerosols. Here, we wish to present our preliminary results on the first-time fabrication of NDs from CWRs and the evaluation of multiple biological properties of these derived nanomaterials for futuristic applications. Advanced-level characterization methods have been carried out to confirm and establish the fabrication of NDs from CWRs. Most importantly, a phytotoxicity bioassay has been performed to determine the toxicity of NDs, and antiviral and antioxidant properties have been evaluated for potential biological applications of the produced NDs. Future research on carbon-based nanomaterials is anticipated to benefit from our research work due to the demand for new antiviral materials, and wider application areas are expected to emerge.

2. EXPERIMENTAL SECTION

2.1. Fabrication of NDs from CWRs. The CWRs were obtained from CSIR-CIMFR, Dhanbad (Jharkhand, India). The methodology adopted to fabricate NDs was almost similar to that described in our previous papers[23,24] with few modifications. Briefly, 50 g of coal reject was mixed with 800 mL of hydrogen peroxide (30%) in a Teflon beaker, and the slurry was subjected to ultrasonic treatment at 20 kHz using a microprocessor-based ultrasonic processor (Model-Power Sonic520) at atmospheric pressure and temperature for 4 h. The resulting slurry solution was then filtered through a 0.22 μm polytetrafluoroethylene membrane after being neutralized by ammonia (8 ml) and further passed through a 1 kDa Millipore kit to obtain the requisite ND suspension filtrate. The dry weight of the NDs sample was found to be approximately 8.62 mg/mL. This solution was concentrated using a rotary evaporator and used for further characterizations and for investigating the phytotoxicity and antioxidant and antiviral properties.

2.2. Characterization of NDs. The structural analysis and elemental mapping of NDs derived from coal rejects were performed on a high-resolution transmission electron microscope (JEM-100 CX II) with a resolution of 1.9−1.4 Å and operated at an accelerating voltage of 60−200 kV. The Image-J software (version: 1.53t) was used to analyze the fast Fourier transform (FFT) and transmission electron microscopy (TEM) images. The functional groups of NDs were analyzed by the Fourier transform infrared (FTIR) spectroscopy in the transmission mode using a PerkinElmer Spectrum Two spectrometer. At first, the sample was prepared by oven-drying in a low temperature range (25−30 °C) and mixed with a KBr pellet thoroughly in an agate mortar, and then, the FTIR spectrum was recorded in the range of 400−4000 cm^{-1}. X-ray photoelectron spectroscopy (XPS) was employed to perform surface chemical analysis of produced NDs. XPS spectra were recorded on a Thermo Scientific ESCALAB Xi+ spectrometer using an Al Kα monochromatic X-ray source at 1486.6 eV and a spherical energy analyzer operating at constant analyzer energy (CAE) mode with the aid of the electromagnetic lens. The optical properties of NDs were investigated by the ultraviolet−visible (UV−vis) and fluorescence (FL) spectroscopy. UV−vis and FL spectra were recorded on UV 1000 LabIndia and HORIBA Fluorolog-3 spectrophotometers. A Laser micro-Raman system (make: HORIBA Jobin Yvon, Model: LabRam HR) was also used to do the Raman analysis.

2.3. Phytotoxicity Studies with NDs. The effect of the ND sample on seed germination and seedling growth was studied on wheatgrass seeds as the model system in water medium. The experiment was carried out following the previously reported protocols with few modifications.[30] The effect was tested for the ND sample over a range of concentrations (10.0, 50.0, 100.0, 200.0, and 300.0 μg/mL). The solution without the test sample (ND) was treated as the control. Fifteen surface sterilized seeds were evenly placed on each Petri dish, added with the aqueous solution of ND and incubated in a controlled environment at 22 ± 1 °C with a photoperiod of 12/12 h light/dark. Each experiment was performed in duplicate. The incubation was continued for 3 days when more than 80% seeds were found to be germinated in the control. Then, the number of germinated seeds and the length of shoot and root were recorded individually. The germination was assessed by a noticeable protrusion (>1 mm) of the radicle through the seed-coat. The radicle and coleoptile were detached carefully from the germinated seeds before measuring their length. The percent inhibition of seed germination and percent growth inhibition were determined as follows

$$\text{inhibition (\%)} = \text{AGC} - \text{AGT/AGC} \times 100\% \quad (1)$$

$$\text{percent growth inhibition (\%)} = \text{ACC} - \text{ACT/ACC} \times 100\% \quad (2)$$

https://doi.org/10.1021/acsomega.2c07981
ACS Omega 2023, 8, 11151−11160

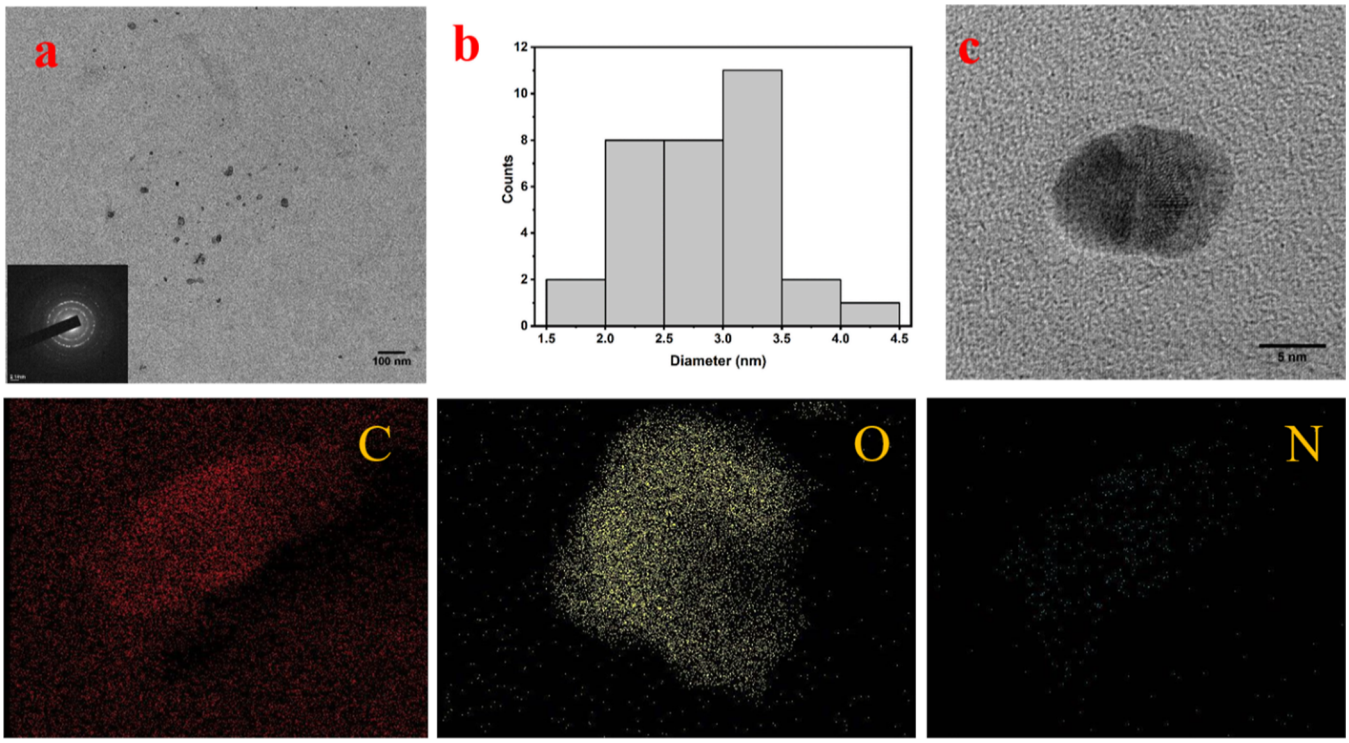

Figure 1. (a) TEM images of the nanocrystals obtained from waste coal (inset: SAED pattern of the nanocrystal which depicts the polycrystalline nature of the obtained ND sample), (b) size distribution image of the carbon nanocrystals, and (c) HR-TEM image of a large size carbon nanocrystal of sizes between 4 and 10 nm. Below are the energy-dispersive spectroscopy images of carbon nanocrystals which mainly consist of carbon, oxygen, and nitrogen.

where AGC denotes the average no. of germinated seeds in control and AGT denotes the average no. of germinated seeds in the test sample and ACC denotes the average length of the coleoptile or radicle in control and ACT denotes the average length of the coleoptile in the treated sample.

2.4. Antiviral Studies with NDs. To evaluate the antiviral activity of the NDs against SARS-CoV2, at first, the cytotoxicity test was carried out using Vero cells via the MTT assay using standard methodology. Here, Vero E6 cells were seeded in the 96-well plates at 80% confluency and treated with various concentrations of the ND sample. A minimum of three experiments with each concentration of ND sample in triplicates were used for the cytotoxicity determination. After 24 h post treatment, MTT was added to each well to a final concentration of 0.5 μg/μL in each well and further incubated for 1 h. Formazan crystals were dissolved in 100 μL/well of DMSO by keeping at 37 °C for 30 min and absorbance was recorded at 540 nM with plate reader. The percent cell viability was calculated from the absorbance of test compound versus negative control. The highest percentage non-cytotoxic concentration was taken forward for assessing their in vitro anti-SARS-CoV2-19 efficacy. Remdisivir, an established Food and Drug Administration (FDA) approved inhibitor of SAR-CoV2, was used as the positive control in the assay. Vero E6 cells seeded in 96 well plates at 80% confluency were infected with SARS-CoV2 that was isolated at an MOI of 0.1 for 2 h. Then, the inoculum was aspirated and fresh media containing different concentration of the ND sample was added to the cells. The NDs exhibiting more than 50% anti-SARS-CoV2 activity was further tested with wider range of concentrations of NDs for IC_{50} determination. After 24 h post-infection, the cells and supernatant were separately subjected to viral RNA isolation followed by qRT-PCR for determining the SARS-CoV2 viral load in the cells (cell associated) and culture supernatants (released virus particles).

2.5. Antioxidant Activity of NDs. Several carbon nanoparticles (NPs) have been reported to exhibit antioxidant properties; therefore, an in vitro antioxidant study was carried out to evaluate the free radicals scavenging activity of the MCQDs using DPPH assay.[31] The principle of the method is based on the fact that in presence of an antioxidant molecule, the marker DPPH (2,2-diphenyl-1-picryl-hydrazyl-hydrate) compound turns from its original purple into pale yellow color which than can be measured as consequent alteration in absorbance using a spectrophotometer compared to untreated negative control. In brief, a series of different concentrations (20−1000 μg/mL) of the ND sample were mixed with 100 μL of methanolic DPPH (125 μM) solution in 96-well plates. The reaction mixtures were incubated in the dark condition for 3 h at 37 °C until measurement of absorbance. The absorbance values were measured at 517 nm in a micro plate reader (EPOCH-2, BioTek, India). All test's data were obtained from triplicate wells of each group carried out in three independent experiments. Ultrapure water (18.2 MΩ cm) and ascorbic acid were used as blank and positive control, respectively.

The percentage of DPPH radical scavenging activity (% RSA) was calculated according to the following formula

$$\%\mathrm{RSA} = \mathrm{absorbance(blank)} - \mathrm{absorbance(test)}/\mathrm{absorbance(blank)} \times 100\% \quad (3)$$

https://doi.org/10.1021/acsomega.2c07981
ACS Omega 2023, 8, 11151−11160

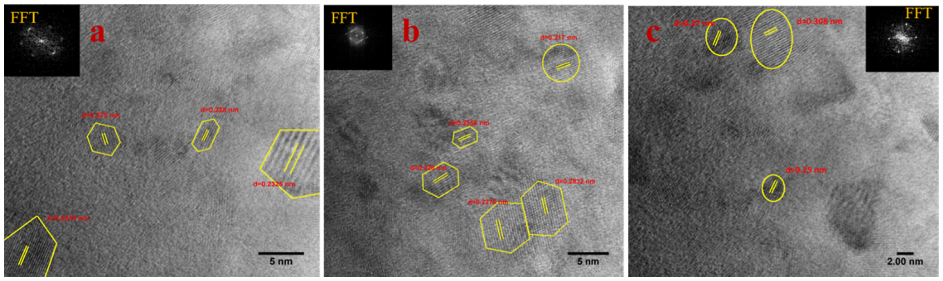

Figure 2. (a) HR-TEM image of the nanocrystal with interplanar spacing between 0.225 and 0.275 nm with inset showing the FFT pattern of the crystalline hexagonal structure, (b) HR-TEM image of the nanocrystal with polycrystalline and monocrystalline domains which are highlighted by hexagons and circles. Inset depicts the crystalline hexagonal FFT pattern. The planar spacing of the crystalline lattices are measured to be between 0.217 and 0.283 nm, (c) HR-TEM image of the nanocrystal with polycrystalline domain which are highlighted by circles with *d*-spacing ranging between 0.25 and 0.308 nm. Inset depicts the FFT pattern of the crystalline structure.

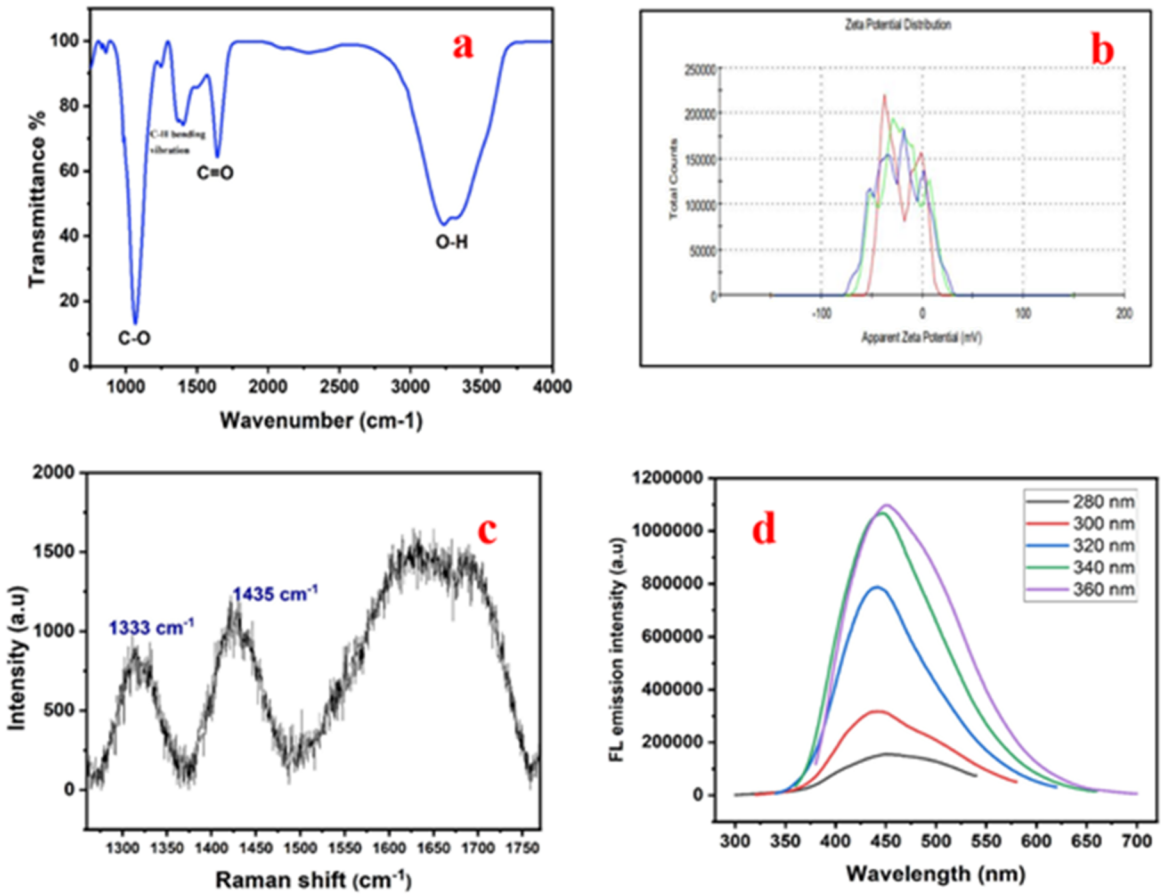

Figure 3. (a) FT-IR spectra of the ND sample showing the C−O, O−H, and C═O vibrational modes, (b) zeta potential analysis of ND indicating good negative results, (c) Raman spectrum, and (d) FL spectra of the ND sample.

3. RESULTS AND DISCUSSION

3.1. Observations from Electron Microscopy Analysis.

The formation of small-sized carbon NPs from coal rejects was confirmed by the TEM image (Figure 1a). Overall, the NPs were uniformly distributed in the thin carbon film of the TEM grid. Some primary particles tended to agglomerate and formed larger-sized secondary particles, presumably on drying during sample preparation. The selected area electron diffraction (SAED) pattern (inset of Figure 1a) confirmed the presence of crystalline phases, typical for coal-derived carbon NDs. The average diameter of these nanocrystals are considered to be between 2 and 3.5 nm (Figure 1b). High-resolution TEM (HR-TEM) analysis was conducted to investigate the crystalline structures of the formed NPs. The HR-TEM image of a large-size NP (Figure 1c) reveals the existence of multiple−crystal planes, confirming the formation of carbon nanocrystals.

The crystalline planes were embedded within amorphous carbon layers, as observed for coal-derived NDs in our earlier study. The elemental mapping images of carbon, oxygen, and nitrogen are also displayed below and this is further confirmed from the XPS elemental studies. For further confirmation of the synthesized nanocrystals, the planar spacing of the lattice fringes were measured from the HR-TEM images of NPs. The interplanar spacing (*d* spacing) of the crystal lattice in the HR-TEM images (Figure 2a−c) reveal that the spacing range lies

https://doi.org/10.1021/acsomega.2c07981
ACS Omega 2023, 8, 11151−11160

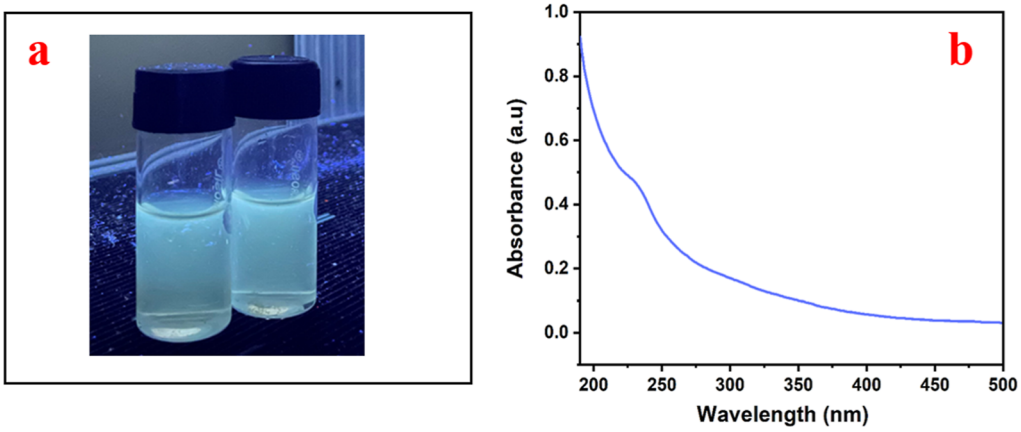

Figure 4. (a) Blue fluorescence under a UV lamp at 365 nm and (b) UV−vis spectrum of the ND depicting a peak at 226 nm.

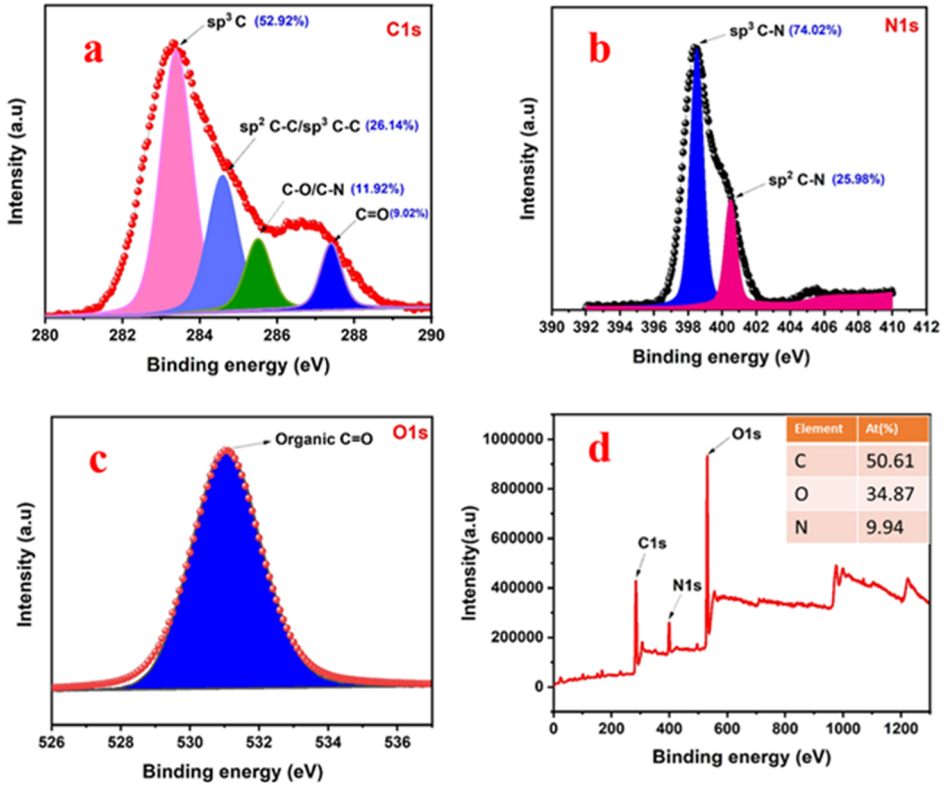

Figure 5. (a) Deconvoluted XPS C 1s spectra of ND depicting the relative atomic percentage of sp^3 and sp^2 hybridized carbon, (b) deconvoluted XPS N 1s spectra of ND depicting the relative atomic percentage of sp^3 and sp^2 hybridized carbon, (c) deconvoluted XPS O1s spectra of ND, and (d) survey spectrum of ND (inset: depicts the elemental atomic percentage of C, O, and N).

between 0.217 and 0.308 nm (2.17−3.08 Å) which indicates the presence of various ND phases. These outcomes are found to be in good concurrence with earlier information on the diamond phases of cubic structures with lattice planes, such as lonsdaleite (hexagonal diamond) (100) (2.18 Å).[24,32] The interplanar *d* spacing of 0.308 nm also confirms the presence of sp^2 hybridized carbon or graphitic carbon, demonstrating that the graphitic layer cannot be completely eliminated by simple oxidation.[33] The particles are seen to be hexagonal (Figure 2a,b) and possess an ordered crystalline structure (Figure 2a−c) in the FFT images (see insets of Figure 2a,c).

3.2. Observations from FT-IR, Raman, FL, UV, XPS, and Zeta Potential Analyses. *3.2.1. FT-IR Spectroscopy.* Surface functional groups are important components of NDs that impact colloidal stability, as well as the chemical, physical, and biological properties of these materials. FTIR spectroscopy was employed to comprehend the surface functionalities of produced NDs. The O−H stretching band at 3235.0 cm^{-1} (see Figure 3a) is directly attributed to hydroxyl groups on NDs.[34] The C═O group is responsible for the prominent absorption peak at approximately 1682 cm^{-1}.[35] The C−H bending vibration is mainly attributed to the absorption peak around 1460 cm^{-1}.[34] The presence of the C−O group is currently indicated by the peak at 1067 cm^{-1}.[36] From Figure 3a, it is discovered that peak intensities of the O−H group predominate over the C═O group peak intensities. As previously noted, the emission intensity thus displays blue fluorescence due to the predominant presence of the O−H

https://doi.org/10.1021/acsomega.2c07981
ACS Omega 2023, 8, 11151−11160

group. The FT-IR spectra confirm the presence of the COOH group on the surface of NDs.

3.2.2. Zeta Potential Analysis. Zeta potential determination is a crucial method for characterizing nanocrystals that may be used to calculate the surface charge and comprehend the physical stability of nanosuspensions. Due to electrostatic interactions that exist between individual particles, nanocrystals with a large positive or negative zeta potential have good physical stability. Herein, the zeta potential of the NDs is found to be −33.3 mV (see Figure 3d) which indicates that the generated NDs are stable when compared to previously reported results.[37] The FT-IR spectra's confirmation of the existence of the COOH group has contributed to the NDs' excellent physical stability.

3.2.3. Raman Analysis. The Raman spectrum mainly here displays three absorption bands. Two distinguishing bands seen in the Raman spectrum at 1435 and 1333 cm^{-1} (see Figure 3b) are located close to the positions of the D-band for sp^3 hybridized carbon framework like 2D hexagonal lattice of graphite cluster.[23] Diamond exhibits well known Raman scattering peak at 1333 cm^{-1}.[26] Numerous studies have demonstrated that the Raman scattering peak of a diamond particle appears at 1333 cm^{-1}.[33] The second peak in the Raman spectra is appearing at 1435 cm^{-1} and this corresponds to the D-band for the carbon with a sp^3 hybridized structure.[38] The G band, which is identified as the third characteristic Raman feature is a broad band observed around 1550−1750 cm^{-1} and is related to the sp^2 structure of carbon[39] (Figure 3b).

3.2.4. Fluorescence Analysis. The FL spectra of the sample containing NDs is displayed in Figure 3c. In a manner similar to that of carbon dots and graphene dots, NDs also exhibit excitation-dependent photoluminescence and this is similar with the reports based on other studies.[40,41] To observe the fluorescence properties at various excitation wavelengths, the ND sample obtained from coal rejects are excited at various excitations ranging from 280−360 nm, at an increment of 20 nm. The maximum emission occurs around 360 nm which implies that fluorescence is produced by electronic transitions which happens within the electronic states of defects found on the surface of diamond crystals and is suited for fluorescence because diamond has a large band gap of 5.49 eV and this is evident from the studies which has been reported earlier.[42,43] As previously observed, the interaction between the carbonyl and hydroxyl groups (OH) $-\pi$ (CO)* may cause the emission dependence on ND excitation.[42]

3.2.5. UV−Vis Analysis. The ND filtrate's vivid bluish green fluorescence under UV light (at 365 nm) is one of its characteristics which is used for studying the antiviral characteristics (see Figure 4a). Figure 4b demonstrates the presence of a UV absorption peak in the filtrate that contains NDs, which is visible between 230 and 250 nm and this denotes the excitation of electrons from π to π^* and n to π^* transition due to the presence of C═C and C═O caused by the oxidation of the diamond surface.[23] A major hump is observed around 226 nm and this is attributed to the intrinsic absorption wavelength λ_{max} of NDs.[42]

3.2.6. XPS Analysis. The chemical structure of the ND sample can be determined from the measured XPS spectra. XPS is very useful to determine the ratio of sp^3 to sp^2 hybridized carbon which helps in the additional verification for the synthesis of ND. Figure 5 shows the peak position and area of the analyses of C 1s, O 1s, and N 1s. Three significant sharp peaks at 284.32, 399.03, and 531.00 eV are shown in the survey spectra and are related to the presence of the elements C, N, and O, respectively. The atomic percentages of the elements of C 1s, O 1s, and N 1s in the survey spectra are 50.61, 34.87, and 9.94%, respectively. C 1s spectra (Figure 5a) are deconvoluted into four peaks at 283.4, 284.6, 285.5, and 287.4 eV which are attributed to sp^3 C,[43] sp^2/sp^3 C−C, C−O/C−N, and C═O,[44] respectively. From the C 1s spectra, the relative atomic percentage of the sp^3 diamond phase is approximately found to be 52.92% and relative content of sp^2 is approximately 26.14%. The N 1s spectra are split into two peaks at 398.5 and 400.5 eV, which are attributed to sp^3 and sp^2 C−N bondings, respectively.[44] Here, the relative percentages of sp^3 and sp^2 C−N bonding are found to be 74.02 and 25.98% which is confirmed from the Figure 5b. Similarly, high-resolution de-convolution XPS spectra of O 1s of coal rejects derived NDs are depicted in Figure 5c. The peak observed at 531.6 eV corresponds to the presence of organic C═O groups.[45] Peaks at 287.4 and 531.6 eV further indicate the development of carboxyl functional groups with higher density on the surface of NDs.[46]

The creation of NDs is a prospective application of ultrasonic therapy with a mechanism that is comparable to the others previously published.[21,24,47] Based on this procedure, many researchers including ours claimed that low-grade coals and atmospheric carbonaceous aerosols might be used to produce blue-fluorescent NDs by using low-power ultrasound waves (40 KHz).[23,24] During ultrasonic treatment, various high temperatures and high pressures are created which could be the starting point in the development of NDs and this may be the speculative process by which NDs are developed from CWRs.[48]

3.3. Evaluation of the Antiviral Properties of NDs. The demand of antiviral drugs and vaccines has intensified with the emergence of Covid-19 viral infection as one of the greatest risks to human health since the 1918 flu pandemic. Despite the fact that about one-third of all infectious disease mortality is due to viruses, still many viral diseases lack specific drugs. The antiviral characteristics of carbon-based nanomaterials have been extensively reported; however, the field is still in its infancy. Considering the precise nanoscale dimensions and forms of viruses, they might also be considered as a form of nanomaterial. For instance, the extremely symmetric nanostructures known as fullerenes exhibit a strong geometric affinity for icosahedral viruses.[49] NPs are without a doubt the most significant nanomaterials that have been studied in nanomedicine and biotechnology so far. Due to flexible manufacturing, biocompatibility, surface tunability, and design of the chemical and structural composition, carbon nanomaterials exhibit low cytotoxicity and specific antiviral activity.[50] Only few reports clearly demonstrate the antiviral activity of NDs, despite research being made extensively on the antiviral activity of other nanomaterials such as carbon quantum dots, graphene, fullerenes, and so forth.[49,50] Here, the primary innovation of our work is the examination of the antiviral properties of NDs made from coal rejects.

The antiviral effect of the synthesized ND sample was evaluated after preliminary cytotoxicity in Vero cells to determine maximum non-toxic concentration. The cytotoxicity of the ND sample was first tested using Vero E6 cells and found to be non-toxic up to the highest tested concentration of 100 μg/mL. The maximum safe dose of 100 μg/mL of ND samples resulted in minimum loss of viability of 5% in the Vero

https://doi.org/10.1021/acsomega.2c07981
ACS Omega 2023, 8, 11151−11160

cells. In order to examine the preliminary antiviral effect at the maximum safe dose, the Vero E6 cells were first infected with SARS-CoV2-l9 for infection; then, the 100 μg/mL ND sample were added to the cells post-infection, and the supernatants were collected at 22 hpi after completion of the treatment period. Following that, the mean C_t was determined through quantitative real-time PCR analysis (shown in Table 1). The

Table 1. Results of Mean C_t Value of the ND Sample When Compared to the C_t Value of the Control

sample	concentration	C_t value	copy number/ML	% inhibition
infection (0.1 mol)		22.168	364688.633	
ND	100 μg/mL	29.859	2322.733	99.3

mean C_t value for NDs obtained by quantitative real time PCR analysis was found to be 29.859 with 99.3% inhibition. This is comparable with the standard drug, Remdisivir with a C_t value of 29.313 with 99.99% reduction. Remdisivir is a FDA approved drug against SARS-CoV-2.

In order to determine the IC_{50} of antiviral activity, the cells were once more treated with various concentrations of ND sample (5, 25, 50, 75, and 100 μg/mL) following similar SARS-CoV-2 infection and treatment protocol (Table 2). The

Table 2. Evaluation Study of the ND Sample against SARS-CoV-2 Virus

Sl. no	compound	concentration (μg/mL)	mean C_t value	copy number/ML	% reduction
1	infected only		27.189	13437.975	
2	ND	5	28.200	6914.347	48.5
3	ND	25	28.707	4954.612	63.1
4	ND	50	28.965	4180.816	68.8
5	ND	75	29.634	2693.913	79.9
6	ND	100	30.830	1226.764	90.8

IC_{50} value of ND for anti-SARS-CoV-2 activity is estimated to be 7.664 μg/mL, which suggest that NDs have reasonably potent antiviral activity. Previous report suggests that the IC_{50} value of Remdisivir against SARS-CoV2 is 4.02 μM (2.42 μg/mL)[16] which is in the comparable range to that of antiviral activity observed in this study. Thus, the antiviral activity of ND against the SARS-CoV-2 is significantly high and comparable to standard FDA approved drug, Remdisivir.

3.4. Evaluation of the Phytotoxicity of NDs. Plants have been utilized as the model system in several research studies investigating various NP kinds, sizes, forms, and concentrations to assess their potential toxicity. Typically, plant toxicity studies are carried out in accordance with well-respected plant bioassays that enable the screening and monitoring of environmental toxins by examining the relationship between the administered dose and the level of caused damage in plants.[51] The effects of NPs on seed germination and root elongation were analyzed in phytotoxicity tests whose results often highlight positive effects, with the extent depending on concentration and size of applied NPs and the plant species tested.[52] Though a dose-dependent inhibition of germination and seedling growth was observed by the synthesized ND in the range of 10.0−300.0 μg/mL, the toxicity showed by ND was very weak (see Figure 6). No detectable influence on the wheatgrass seed germination was observed up to 200.0 μg/mL and only 7.7% inhibition was obtained at 300.0 μg/mL.

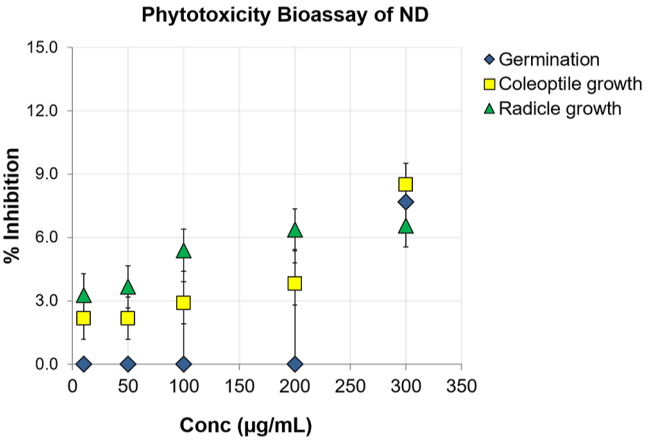

Figure 6. Water medium phytotoxicity (wheatgrass) bioassay of ND in the concentration range 10.0−300.0 μg/mL.

The coleoptile and radicle growth inhibition at 100.0 μg/mL was less than 6% which was less than 9% even at 300.0 μg/mL. The results recommended a safe use of these synthesized NDs from waste coal on plants up to 300.0 μg/mL in the aqueous medium. This is comparable with the previously published results on other NPs.[53] In a previous study, toxicity assessment demonstrated that detonation synthesis-based NDs did not affect the photosynthetic process in wheat plants under illumination.[54] In a recent report, pre-sowing treatment of the Chinese cabbage seeds by aqueous suspension of detonation NDs (enriched with boron impurities) showed positive effect on the germination and early stage of development.[55] These studies taken together indicate that the fabricated NDs from coal rejects are the safe and futuristic materials for agricultural applications.

3.5. Evaluation of Antioxidant Activity of NDs. In the biological system, generation of reactive oxygen species or free radicals is a critical phenomenon which has been showed to be altered by NPs with antioxidant activity.[56] As it is already known that carbon NPs have good semiconductor property with the capability to transfer or receive an electron, which implies them as potent candidate for manipulation of ROS in a biological system.[56] 1,1-diphenyl-2-picryl-hydrazyl ($DPPH^{\bullet}$) radical scavenging is a commonly used method for evaluating the antioxidant activity. Seven different concentrations of ND samples were tested ranging from 20 to 1000 μg/mL via the ($DPPH^{\bullet}$) radical scavenging method. Figure 7 clearly shows that % of RSA gradually increased corresponding to the increase in concentration of the ND sample.

Though the RSA of ND is relatively low in comparison to the positive control, there is a clear indication of dose-dependent radical scavenging with the ND sample. The mechanism can be based on the deprotonation of the hydrogen atom from NDs' surface functional groups (−OH and −COOH) toward DPPH molecules to make them a stable compound. This phenomenon results in free radicals on the NP surface, which could be stabilized by the rearrangement of functional groups among themselves or through resonance of unpaired electrons.[57] Here, our results clearly suggest that there are reasonable antioxidant properties of the CWR-

https://doi.org/10.1021/acsomega.2c07981
ACS Omega 2023, 8, 11151−11160

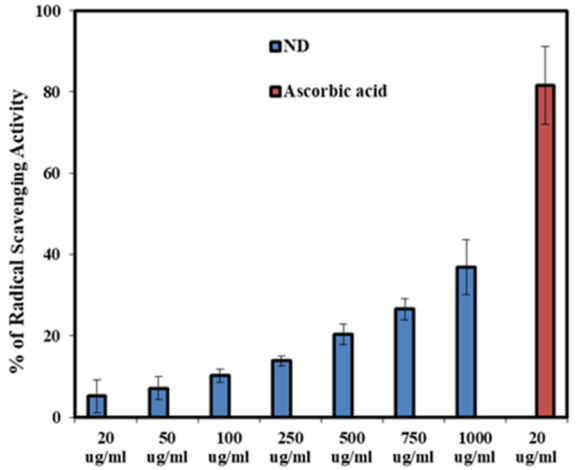

Figure 7. Percentage of % RSA of ND sample was calculated against the concentration used in the experiment.

derived NDs and could have wide implications in future biological and therapeutic applications of NDs. Furthermore, specific detailed in vitro and in vivo studies are necessary for better understanding of the antioxidant effects and its correlation with antiviral and other biological activities.

4. SUMMARY

In summary, for the first time, NDs of significant value have been produced simply from CWRs by employing a wet-chemical technique with ultrasonic assistance in the presence of H_2O_2. The HR-TEM, FFT patterns, XPS, Raman spectroscopy, zeta potential studies confirm the formation of NDs from coal rejects. The coal rejects derived NDs had promising antiviral activity against SARS-CoV-2 virus with a mean C_t value of 29.859 with 99.3% inhibition, which are comparable to the FDA approved Remdisivir antiviral drug. The synthesized NDs are also safe toward plants up to 300 μg/mL without causing any significant toxicological effect or phytotoxicity. A moderate level of dose-dependent free radical scavenging activity is also observed for the synthesized NDs, indicating the presence of reasonable antioxidant properties. Thus, this study creates new prospects for producing non-toxic NDs for therapeutic and other biological applications using coal rejects, providing a new paradigm for converting coal-derived wastes into wealth.

AUTHOR INFORMATION

Corresponding Author

Binoy K. Saikia − *Coal and Energy Division, CSIR-North East Institute of Science and Technology, Jorhat 785006 Assam, India; Academy of Scientific and Innovative Research (AcSIR), Ghaziabad 201002, India;* orcid.org/0000-0002-3382-6218; Email: bksaikia@neist.res.in, bksaikia@gmail.com

Authors

Anusuya Boruah − *Coal and Energy Division, CSIR-North East Institute of Science and Technology, Jorhat 785006 Assam, India; Academy of Scientific and Innovative Research (AcSIR), Ghaziabad 201002, India*

Kallol Roy − *Biological Science & Technology Division, CSIR-North East Institute of Science and Technology, Jorhat 785006 Assam, India; Academy of Scientific and Innovative Research (AcSIR), Ghaziabad 201002, India*

Ashutosh Thakur − *Coal and Energy Division, CSIR-North East Institute of Science and Technology, Jorhat 785006 Assam, India; Academy of Scientific and Innovative Research (AcSIR), Ghaziabad 201002, India*

Saikat Haldar − *Agrotechnology and Rural Development Division, CSIR-North East Institute of Science and Technology, Jorhat 785006 Assam, India; Academy of Scientific and Innovative Research (AcSIR), Ghaziabad 201002, India;* orcid.org/0000-0002-5968-5230

Rituraj Konwar − *Biological Science & Technology Division, CSIR-North East Institute of Science and Technology, Jorhat 785006 Assam, India; Academy of Scientific and Innovative Research (AcSIR), Ghaziabad 201002, India*

Prasenjit Saikia − *Coal and Energy Division, CSIR-North East Institute of Science and Technology, Jorhat 785006 Assam, India; Academy of Scientific and Innovative Research (AcSIR), Ghaziabad 201002, India*

Complete contact information is available at: https://pubs.acs.org/10.1021/acsomega.2c07981

Notes

The authors declare no competing financial interest.

ACKNOWLEDGMENTS

Authors are thankful to the Director, CSIR-NEIST, for his keen interest to this research field and his permission to publish the paper. The fund received from CSIR (OLP-2059) is thankfully acknowledged. Institute of Life Sciences (ILS), Bhubaneswar (India) is duly acknowledged for the antiviral testing. The comments received from the three anonymous reviewers are useful for improving the revision.

REFERENCES

(1) Boruah, A.; Saikia, B. K. Chemical Fabrication of Efficient Blue-luminescent Carbon Quantum Dots from Coal Washery Rejects (Waste) for Detection of Hg2+ and Cr6+ Ions in water. *ChemistrySelect* **2022**, *7*, No. e202104567.

(2) Zhu, Y.; Li, J.; Li, W.; Zhang, Y.; Yang, X.; Chen, N.; Sun, Y.; Zhao, Y.; Fan, C.; Huang, Q. The Biocompatibility of NDs and Their Application in Drug Delivery Systems. *Theranostics* **2012**, *2*, 302−312.

(3) Gibson, N.; Shenderova, O.; Luo, T. J. M.; Moseenkov, S.; Bondar, V.; Puzyr, A.; Purtov, K.; Fitzgerald, Z.; Brenner, D. W. Colloidal stability of modified nanodiamond particles. *Diam. Relat. Mater.* **2009**, *18*, 620−626.

(4) Vlasov, I. I.; Shiryaev, A. A.; Rendler, T.; Steinert, S.; Lee, S. Y.; Antonov, D.; Vörös, M.; Jelezko, F.; Fisenko, A. V.; Semjonova, L. F.; Biskupek, J.; Kaiser, U.; Lebedev, O. I.; Sildos, I.; Hemmer, P. R.; Konov, V. I.; Gali, A.; Wrachtrup, J. Molecular-sized fluorescent nanodiamonds. *Nat. Nanotechnol.* **2014**, *9*, 54−58.

(5) Howard, T. H. Diamond Synthesis. U.S. Patent 2,947,608 A, August 2, 1960.

(6) Wang, H.; Cui, Y. I. Nanodiamonds for energy. *Carbon Energy* **2019**, *1*, 13−18.

(7) Qin, J. X.; Yang, X. G.; Lv, C. F.; Li, Y. Z.; Chen, X. X.; Zhang, Z. F.; Zang, J. H.; Yang, X.; Liu, K. K.; Dong, L.; Shan, C. X. Humidity sensors realized via negative photoconductivity effect in NDs. *J. Phys. Chem. Lett.* **2021**, *12*, 4079−4084.

(8) Huang, T. S.; Tzeng, Y.; Liu, Y. K.; Chen, Y. C.; Walker, K. R.; Guntupalli, R.; Liu, C. Immobilization of antibodies and bacterial binding on nanodiamond and carbon nanotubes for biosensor applications. *Diam. Relat. Mater.* **2004**, *13*, 1098−1102.

(9) Puthongkham, P.; Venton, B. J. Nanodiamond Coating Improves the Sensitivity and Antifouling Properties of Carbon-Fiber Microelectrodes. *ACS Sens.* **2019**, *4*, 2403−2411.
(10) Raina, A.; Irfan Ul Haq, M. I. U.; Anand, A.; Mohan, S.; Kumar, R.; Jayalakshmi, S.; Arvind Singh, R. A. Nanodiamond Particles as Secondary Additive for Polyalphaolefin Oil Lubrication of Steel-Aluminium Contact. *Nanomaterials* **2021**, *11*, 1438.
(11) Chan, J. X.; Wong, J. F.; Petrů, M.; Hassan, A.; Nirmal, U.; Othman, N.; Ilyas, R. A. Effect of Nanofillers on Tribological Properties of Polymer Nanocomposites: A Review on Recent Development. *Polymers* **2021**, *13*, 2867.
(12) Katzensteiner, A.; Rosalie, J. M.; Pippan, R.; Bachmaier, A. Synthesis of nanodiamond reinforced silver matrix nanocomposites: microstructure and mechanical properties. *Mater. Sci. Eng., A* **2020**, *782*, 139254.
(13) Chauhan, S.; Jain, N.; Nagaich, U. Nanodiamonds with powerful ability for drug delivery and biomedical applications: Recent updates on in vivo study and patents. *J. Pharm. Anal.* **2020**, *10*, 1−12.
(14) Zhang, W.; Patel, K.; Schexnider, A.; Banu, S.; Radadia, A. D. Nanostructuring of biosensing electrodes with nanodiamonds for antibody immobilization. *ACS Nano* **2014**, *8*, 1419−1428.
(15) Dolmatov, V. Y. Detonation-synthesis NDs: synthesis, structure, properties and applications. *Russ. Chem. Rev.* **2007**, *76*, 339.
(16) Li, L.; Liu, L.; Wei, W.; Song, S.; Wei, W.; Wee, T. S. W. Controllable Synthesis of Graphene by Plasma-Enhanced Chemical Vapor Deposition and Its Related Applications. *Adv. Sci.* **2016**, *3*, 1600003.
(17) Kumar, A.; Ann Lin, P. L.; Xue, A.; Hao, B.; Khin Yap, Y.; Sankaran, R. M. Formation of nanodiamonds at near-ambient conditions via microplasma dissociation of ethanol vapour. *Nat. Commun.* **2013**, *4*, 2618.
(18) Welz, S.; Gogotsi, Y.; McNallan, J. M. Nucleation, growth, and graphitization of diamond nanocrystals during chlorination of carbides. *J. Appl. Phys.* **2003**, *93*, 4207.
(19) Daulton, T. L.; Kirk, M. A.; Lewis, R. S.; Rehn, L. E. Production of NDs by high-energy ion irradiation of graphite at room temperature. *Nucl. Instrum. Methods Phys. Res., Sect. B* **2001**, *175*−*177*, 12−20.
(20) Amans, D.; Chenus, A. C.; Ledoux, G.; Dujardin, C.; Reynaud, C.; Sublemontier, O.; Masenelli-Varlot, K. M.; Guillois, O. Nanodiamond synthesis by pulsed laser ablation in liquids. *Diam. Relat. Mater.* **2009**, *18*, 177−180.
(21) Khachatryan, A. Kh.; Aloyan, S. G.; May, P. W.; Sargsyan, R.; Khachatryan, V. A.; Baghdasaryan, V. S. Graphite-to-diamond transformation induced by ultrasound cavitation. *Diam. Relat. Mater.* **2008**, *17*, 931−936.
(22) Liu, T.; Yang, X. G.; Li, Z.; Hu, Y. W.; Lv, C. F.; Zhao, W. B.; Zang, J. H.; Shan, C. X. Two-step high-pressure high-temperature synthesis of NDs from naphthalene. *Chin. Phys. B* **2020**, *29*, 108102.
(23) Islam, N.; Dihingia, A.; Manna, P.; Das, T.; Kalita, J.; Dekaboruah, H. P.; Saikia, B. K. Environmental and toxicological assessment of nanodiamond-like materials derived from carbonaceous aerosols. *Sci. Total Environ.* **2019**, *679*, 209−220.
(24) Das, T.; Saikia, B. K. Nanodiamonds produced from low grade Indian Coals. *ACS Sustainable Chem. Eng.* **2017**, *5*, 9619−9624.
(25) Das, T.; Saikia, B. K.; Dekaboruah, H. P.; Bordoloi, M.; Neog, D.; Bora, J. J.; Lahkar, J.; Narzary, B.; Roy, S.; Ramaiah, D. Blue-fluorescent and biocompatible carbon dots derived from abundant low-quality coals. *J. Photochem. Photobiol., B* **2019**, *195*, 1−11.
(26) Lueking, A. D.; Gutierrez, H. R.; Fonseca, D. A.; Narayanan, D. L.; Van Essendelft, D. V.; Jain, P.; Clifford, C. E. B. Combined Hydrogen Production and Storage with Subsequent Carbon Crystallization. *J. Am. Chem. Soc.* **2006**, *128*, 7758−7760.
(27) Lueking, A. D.; Gutierrez, H. R.; Jain, P.; Van Essandelft, D. T.; Burgess-Clifford, C. E. The effect of HCl and NaOH treatment on structural transformations in a ball-milled anthracite after thermal and chemical processing. *Carbon* **2007**, *45*, 2297−2306.
(28) Sun, Y.; Kvashnin, A. G.; Sorokin, P. B.; Yakobson, B. I.; Billups, W. E. Radiation-Induced Nucleation of Diamond from Amorphous Carbon: Effect of Hydrogen. *J. Phys. Chem. Lett.* **2014**, *5*, 1924−1928.
(29) Xiao, J.; Liu, P.; Yang, G. W. Nanodiamonds from coal at ambient conditions. *Nanoscale* **2015**, *7*, 6114−6125.
(30) Mahanta, B. P.; Kemprai, P.; Bora, P. K.; Lal, M.; Haldar, S. Phytotoxic essential oil from black turmeric (Curcuma caesia Roxb.) rhizome: Screening, efficacy, chemical basis, uptake and mode of transport. *Ind. Crops Prod.* **2022**, *180*, 114788.
(31) Blois, M. S. Antioxidant determinations by the use of a stable free radical. *Nature* **1958**, *181*, 1199−1200.
(32) Hao, J.; Pan, L.; Gao, S.; Fan, H.; Gao, B. Production of fluorescent nano-diamonds through femtosecond pulsed laser ablation. *Opt. Mater. Express* **2019**, *9*, 4734−4741.
(33) Kumar, V.; Srivastava, A. K.; Toyoda, S.; Kaur, I. Extraction of low toxicity NDs from carbonaceous wastes. *Fullerenes, Nanotubes, Carbon Nanostruct.* **2016**, *24*, 190−194.
(34) Petit, T.; Puskar, L. FTIR spectroscopy of NDs: Methods and interpretation. *Diam. Relat. Mater.* **2018**, *89*, 52−66.
(35) Karaveli, S.; Gaathon, O.; Wolcott, A.; Sakakibara, R.; Shemesh, D. S.; Peterka, E. S.; Boyden, J. S.; Owen, R.; Yuste, D.; Englund, D. Modulation of nitrogen vacancy charge state and fluorescence in NDs using electrochemical potential. *Proc. Natl. Acad. Sci. U. S. A.* **2016**, *113*, 3938−3943.
(36) Wolcott, A.; Schiros, T.; Trusheim, M. E.; Chen, E. H.; Nordlund, D.; Diaz, R. E.; Gaathon, O.; Englund, D.; Owen, J. S. Surface structure of aerobically oxidized diamond nanocrystals. *J. Phys. Chem. C* **2014**, *118*, 26695−26702.
(37) Ge, G.; Wang, Y. Estimation of Nanodiamond Surface Charge Density from Zeta Potential and Molecular Dynamics Simulations. *J. Phys. Chem. B* **2017**, *121*, 3394−3402.
(38) Osswald, S.; Mochalin, V. N.; Havel, M.; Yushin, G.; Gogotsi, Y. Phonon confinement effects in the Raman spectrum of nanodiamond. *Phys. Rev. B: Condens. Matter Mater. Phys.* **2009**, *80*, 075419.
(39) Mermoux, M.; Chang, S.; Girard, H.; Arnault, J. C. Raman spectroscopy study of detonation nanodiamond. *Diam. Relat. Mater.* **2018**, *87*, 248−260.
(40) Baker, S. N.; Baker, G. A. Luminescent carbon nanodots: emergent nanolights. *Angew. Chem., Int. Ed.* **2010**, *49*, 6726−6744.
(41) Shen, J.; Zhu, Y.; Yang, X.; Li, C. Graphene quantum dots: emergent nanolights for bioimaging, sensors, catalysis, and photovoltaic devices. *Chem. Commun.* **2012**, *48*, 3686−3699.
(42) Shenderova, O. A.; Shames, A. I.; Nunn, N. A.; Torelli, M. D.; Vlasov, I.; Zaitsev, A. Review Article: Synthesis, properties, and applications of fluorescent diamond particles. *J. Vac. Sci. Technol., B: Nanotechnol. Microelectron.: Mater., Process., Meas., Phenom.* **2019**, *37*, 030802.
(43) Humbert, B.; Hellala, N.; Ehrhardt, J. J.; Barrat, S.; Bauer-grosse, E. X-ray photoelectron and Raman studies of microwave Plasma Assisted Chemical Vapour Deposition (PACVD) diamond films. *Appl. Surf. Sci.* **2008**, *254*, 6400−6409.
(44) Zhao, M.; Cao, Y.; Liu, X.; Deng, J.; Li, D.; Gu, H. Effect of nitrogen atomic percentage on N+ -bombarded MWCNTs in cytocompatibility and hemocompatibility. *Nanoscale Res. Lett.* **2014**, *9*, 142.
(45) Lim, D. G.; Kim, K. H.; Kang, E.; Lim, S. H.; Ricci, J.; Sung, S. K.; Kwon, M. T.; Jeong, S. H. Comprehensive evaluation of carboxylated nanodiamond as a topical drug delivery system. *Int. J. Nanomed.* **2016**, *11*, 2381−2395.
(46) Fujimoto, A.; Yamada, Y.; Koinuma, M.; Sato, S. Origins of sp3 C peaks in C1s X-ray photoelectron spectra of carbon materials. *Anal. Chem.* **2016**, *88*, 6110−6114.
(47) Zhen-Xia, W.; Qiang-Yan, P.; Jian-Gang, H.; Zhen-Zhong, Y.; Yong-Qing, H.; Zhi-Yuan, Z. Synthesis of diamond nanocrystals by double ions (40Ar+,C2H6+) bombardment. *Wuli Xuebao* **2007**, *56*, 4829−4833.
(48) Saikia, B. K.; Dutta, A. M.; Saikia, L.; Ahmed, S.; Baruah, B. P. Ultrasonic assisted cleaning of high sulphur Indian coals in water and mixed alkali. *Fuel Process. Technol.* **2014**, *123*, 107−113.

https://doi.org/10.1021/acsomega.2c07981
ACS Omega 2023, 8, 11151−11160

(49) Dechant, P. P.; Wardman, J.; Keef, T.; Twarock, R. Viruses and fullerenes–symmetry as a common thread. *Acta Crystallogr., Sect. A: Found. Adv.* **2014**, *70*, 162−167.
(50) Pinna, A.; Ricco', L.; Migheli, G.; Rocchitta, R.; Serra, S.; Falcaro, G.; Malfatti, R.; Innocenzi, P. A.; Innocenzi, P. A MOF-based carrier for in situ dopamine delivery. *RSC Adv.* **2018**, *8*, 25664−25672.
(51) Grant, W. F. The present status of higher plant bioassays for the detection of environmental mutagens. *Mutat. Res., Fundam. Mol. Mech. Mutagen.* **1994**, *310*, 175−185.
(52) Giorgetti, L. Effects of Nanoparticles in Plants: Phytotoxicity and Genetoxicity Assessment. In *Nanomaterials in Plants Algae and Microorganisms*; Tripathi, D. K., Ahmad, P., Sharma, S., Chauhan, D., Dubey, N. K., Eds.; 1st ed.; Academic press, 2019; pp 65−87.
(53) Adhikari, T.; Kundu, S.; Biswas, A. K.; Tarafdar, J. C.; Rao, A. S. Effect of copper oxide nanoparticle on seed germination of selected crops. *J. Agric. Sci. Technol.* **2012**, *2*, 815−823.
(54) Chernysheva, M. G.; Myasnikov, I. Y.; Badun, G. A.; Matorin, D. N.; Gabbasova, D. T.; Konstantinov, A. I.; Korobkov, V. I.; Kulikova, N. A. Humic substances alter the uptake and toxicity of nanodiamonds in wheat seedlings. *J. Soils Sediments* **2018**, *18*, 1335−1346.
(55) Shilova, O. A.; Dolmatov, V. Y.; Panova, G.; Khamova, T. V.; Baranchikov, A. E.; Gorshkova, Y.; Udalova, O.; Zhuravleva, A. S.; Kopitsa, G. P. Nanodiamond Batch Enriched with Boron: Properties and Prospects for Use in Agriculture. *Biointerface Res. Appl. Chem.* **2022**, *12*, 6134−6147.
(56) Pandey, A. K.; Bankoti, K.; Nath, T. K.; Dhara, S. Hydrothermal Synthesis of Clove Buds-Derived Multifunctional Carbon Dots Passivated with PVP- Antioxidants, Catalysis, and Bioimaging Applications. *Colloids Surf., B* **2021**, *220*, 112926.
(57) Rodríguez-Varillas, S.; Fontanil, T.; Obaya, Á.J.; Fernández-González, A.; Murru, C.; Badía-Laíño, R. Biocompatibility and Antioxidant Capabilities of Carbon Dots Obtained from Tomato (Solanum lycopersicum). *Appl. Sci.* **2022**, *12*, 773.

https://doi.org/10.1021/acsomega.2c07981
ACS Omega 2023, 8, 11151−11160